Late Quaternary slip rate gradient defined using high-resolution topography and ^{10}Be dating of offset landforms on the southern San Jacinto Fault zone, California

Kimberly Blisniuk[1], Thomas Rockwell[2], Lewis A. Owen[3], Michael Oskin[1], Caitlin Lippincott[2], Marc W. Caffee[4], Jason Dortch[3]

[1]Department of Geological Sciences, University of California, Davis, CA 95616 USA

[2]Department of Geological Sciences, San Diego State University, San Diego, CA 92182, USA

[3]Department of Geology, University of Cincinnati, Cincinnati, OH 45221, USA

[4]Department of Physics, Purdue University, West Lafayette, IN 47906, USA

Recent studies suggest the San Jacinto fault zone may be the dominant structure accommodating PA-NA relative plate motion. However, because the late Quaternary slip history of the southern San Andreas fault system is insufficiently understood, it is difficult to evaluate the partitioning of deformation across the plate boundary and its evolution. Landforms displaced by the Clark fault of the southern San Jacinto fault zone were mapped using high-resolution airborne laser-swath topography and selected offset landforms were dated using cosmogenic ^{10}Be. Beheaded channels at Rockhouse Canyon, displaced by 500 ±70 m and 220 ±70 m, have been dated to 47 ±8 ka and 28 ±9 ka, respectively. Farther south, near the southern Santa Rosa Mountains, an alluvial deposit displaced by 51 ±9 m has been dated to 35 ±7 ka. From these sites, the slip rate of the Clark fault is determined to diminish southward from 8.9 ±2.0 to 1.5 ±0.4 mm/yr. This implies a slip-rate decrease along the Clark fault from Anza southeastward to its surface termination near the Salton Trough, where slip is transferred to the Coyote Creek fault, and additional

deformation is compensated by folding and thrusting in the basin. These data suggest that since ~30 to 50 ka, the slip rate along the southern San Jacinto fault zone has been lower than, or equivalent to, the rate along the southernmost San Andreas fault. Accordingly, either the slip rate of the San Jacinto fault has substantially decreased since fault initiation, or fault slip began earlier than previously suggested.

1. INTRODUCTION

[1] To the south of the Big Bend at approximately 34°5'N latitude in southern California, the San Andreas fault system consists of the southern San Andreas, San Jacinto, and Elsinore fault zones (Fig. 1). The southern San Andreas and the San Jacinto fault zones (SJFZ) are the two principal structures, together accommodating ~35 mm/yr, that is ~80%, of the Pacific-North America (PA-NA) relative plate motion in this region [*King and Savage*, 1983; *DeMets and Dixon*, 1999; *Bennett et al*., 2004; *Fialko*, 2006]. Geodetically derived slip rate estimates are on the order of 10-20 mm/yr for both of these fault zones, but only 2-6 mm/yr for the Elsinore fault zone [*Johnson et al*., 1994; *Bennett et al*., 1996; *Meade and Hager*, 2005; *Becker et al*., 2005; *Fay and Humphreys*, 2005].

[2] The SJFZ has historically been more seismically active than the southern San Andreas fault zone [*Thatcher et al*., 1975; *Richards-Dinger and Shearer*, 2006], but its longer-term slip history is controversial. Although many previous studies across the fault system have documented well-preserved offsets of Quaternary landforms [e.g *Sharp*, 1967; *Sharp*, 1981; *Rockwell et al*., 1990], fault slip rates are often more poorly defined due to the inherent difficulties of dating Quaternary deposits. Moreover, the offsets that

have been dated span time scales ranging from 10^3 to 10^6 years, complicating direct comparison of slip rates over comparable periods for the San Jacinto and the San Andreas fault zones [*Sharp*, 1981; *Weldon and Sieh*, 1985; *Morton and Matti*, 1986; *Harden and Matti*, 1989; *Rockwell et al*., 1990]. Variation in published slip rates may be resolved by a kinematic model of codependent slip histories for these fault zones [e.g. *Sharp*, 1981; *Bennett et al*., 2004]. Alternatively, along-strike gradient in slip rate could account for the variety of slip rates measured along these fault zones without need for temporal variation.

[3] Presently, there are no slip rate estimates from ^{10}Be exposure dating of offset landforms along the SJFZ, but the utility of this method has been demonstrated by recent work along the San Andreas fault [*Matmon et al*., 2005; *van der Woerd et al*., 2006]. Due to the excellent preservation of offset landforms in the arid Anza Borrego desert of southern California, the SJFZ provides an ideal location for surface exposure dating. Additionally, the availability of high resolution laser swath mapping [*Bevis et al.*, 2005] makes the SJFZ an outstanding candidate for studying the distribution of strain within a nascent strike-slip fault system [*Oskin et al.*, 2007]. In this paper, we present the first late Quaternary slip rates from ^{10}Be dating of landforms displaced along the central and southern Clark fault segment of the SJFZ, at Rockhouse Canyon and the southern Santa Rosa Mountains, respectively (Fig. 2). We integrate these newly determined slip rates with previously published slip rate estimates for the northern segment and with total bedrock displacement to make inferences on the long-term slip rate history of the SJFZ and its implication to earthquake recurrence models used in assessing seismic hazards in southern California.

2. Tectonic Setting:

[4] The ~230 km long SJFZ extends from the Big Bend of the San Andreas fault southward with an average strike of ~N45°W (Fig. 1). In the central and southern SJFZ, the two most active strands are the roughly parallel Coyote Creek and Clark fault, both ~60 km long and located ~10 km apart (Fig. 2). Deformation is partitioned between these two strands displaying numerous active features that offset and fold Cretaceous tonalites, meta-tonalites, cataclasites, and Quaternary surfaces along the fault and adjacent to the fault (Fig. 2) [*Sharp*, 1967]. Landforms along the ~120 km long Clark fault strand suggests that it is the dominant strand in accommodating slip of the southern SJFZ. The right-lateral strike-slip behavior of the Clark fault strand terminates southeast of the Santa Rosa Mountains into a zone of diffuse faulting and folding in the northwestern Imperial Valley [*Sharp*, 1981; *Kirby, et al.*, 2007]. Quaternary features along the Clark fault strand that indicate youthful activity include folds, offset and deformed terraces, deflected channels, beheaded channels, offset surfaces, fault scarps, and linear ridges.

[5] Total bedrock displacement along the northern and central section of the SJFZ is ~22 to 24 km [*Sharp*, 1967] based on offset of the Thomas Mountain sill in contact with metamorphic rocks of the Bautista Complex (Fig. 2) [*Sharp*, 1967]. Farther south toward Rockhouse Canyon and the southern Santa Rosa Mountains, Cretaceous tonalite, metamorphic rocks, and the eastern Peninsular Ranges cataclastic and mylonitic zones are displaced by ~14.5 km (Fig. 2) [*Sharp*, 1967], and these same zones are displaced ~3.5 to 4.8 km by the adjacent Coyote Creek fault strand (Fig.2) [*Sharp*, 1967; *Janecke et al.*, 2008].

[6] Inception of the SJFZ as a major right-lateral strike slip fault zone has variably

been inferred to have occurred as early as ~2.4 Ma based on a slip rate of 10 mm/yr [Sharp, 1981; Rockwell et al., 1990] and a total offset of 24 km [*Sharp*, 1967], to 1.5 Ma [*Morton and Matti*, 1993], to as recently as ~1.1 Ma [*Lutz et al.*, 2006; *Kirby et al.*, 2007]. From the northern SJFZ, *Morton and Matti* [1993] suggest an initiation age of 1.5 Ma from sedimentologic changes in the upper San Timoteo Formation deposited adjacent to the SJFZ, dated by a rodent tooth fossil identified as *Microtus Californicus*. In the central SJFZ, using the best-estimated late Quaternary slip rate of 10-14 mm/yr [*Rockwell et al.*, 1990], one can infer an inception age of 1.7-2.4 Ma based on the 24 km of bedrock displacement, although this assumes the slip rate has been fairly constant since inception. For the southern SJFZ, a 1.05-1.07 Ma initiation age has been suggested based on dramatic changes in basin dynamics inferred from sedimentary rocks [*Lutz et al.*, 2006; *Kirby et al.*, 2007]. Based on a magnetic reversal located between two non-conformable stratigraphic units, the Ocotillo and Borrego Formations, the initial progradation of sediment beginning at ~1.1 Ma is interpreted as evidence for initiation of faults in the Salton Trough [*Lutz et al.*, 2006; *Kirby et al.*, 2007].

[7] Published mid-to-late Quaternary slip rate estimates along the SJFZ are also quite variable. Along the Clark fault strand at Anza, *Sharp* [1981] estimated a minimum mid-Quaternary to present slip rate of 8-12 mm/yr by reconstructing monolithologic alluvial fan deposits to their source (Fig. 2 and Table 1). Southward, along the Coyote Creek fault strand, a mid-Quaternary to present rate of 10 ± 3 mm/yr has been suggested from clasts displaced ~6 km from their source [*Dorsey*, 2002]. However, the offset by *Dorsey* [2002] 1) does not account for possible along-fault transport of these clasts, which would lower the amount of slip and 2) is greater than the total bedrock offsets of

4.8 km and 3.5 km inferred by *Sharp* [1967] and *Janecke et al.* [2008], respectively; it thus likely represents an upper limit for the mid-Quaternary slip rate of the Coyote Creek fault strand. For the late Quaternary, along the northern section of the SJFZ, in the San Timoteo badlands, a horizontal slip rate of at least 20 mm/yr was indirectly estimated from luminescence dating of uplifted terraces along a restraining bend in the fault; this estimate was obtained combining terrace uplift rates with an elastic-half space model of deformation [Table 1; *Kendrick et al.*, 2002]. In contrast to a fast slipping northern SJFZ, *Wesnousky et al.* [1991] used ^{14}C and an offset channel margin to determine a minimum latest Holocene rate of 1.7-3.3 mm/yr from what is considered the main strand of multiple fault strands. The only late Quaternary slip rates published on the central section of the SJFZ are from the Clark fault strand near Anza [*Rockwell et al.*, 1990]. Based on ^{14}C dating of an offset fan deposit *Rockwell et al.* [1990] obtained a slip rate of >9 ± 2 mm/yr since 9.5 ka. Using soil development on offset alluvial deposits, they determined slip rates of 11 $^{+9}/_{-5}$ mm/yr since ~14 ka, 12 $^{+9}/_{-5}$ mm/yr since ~17 ka, and 13 $^{+10}/_{-6}$ mm/yr since ~48 ka. Additionally, a long paleoseismic record from Anza at Hog Lake shows that earthquakes recur frequently and are strongly clustered in time [*Rockwell et al.*, 2006]. Based on ^{14}C ages and paleoseismic investigations, *Rockwell et al.* [2006] and *Rockwell* [2008] estimate a late Holocene slip rate of 12-15 mm/yr by combining an average return period of ~230 years over the past 4000 years with surface displacement from the last two ruptures at Anza (3-4 m per event).

[8] Different geodetic models of strain accumulation across the southern SJFZ also imply a wide range of slip rate estimates. Block models of GPS data from the southern SJFZ indicate slip rates of 9-15 mm/yr [Table 1; *Bennett et al.*, 1996; *Becker et*

al., 2005; *Meade and Hager,* 2005], which is consistent with a 14-15 mm/yr slip rate estimate inferred from elastic and viscoelastic models of crustal deformation [Table 1; *Fay and Humphreys,* 2005]. In contrast, the results of a study by *Fialko* [2006], combining interferometric satellite synthethic aperature radar (InSAR) data with an elastic deep slipping SJFZ suggest a slip rate of 21 ± 1 mm/yr along the southern part of the fault zone, although this rate probably includes the strain accommodated by folding and NE-striking cross-faults. Similarly high rates are implied by more recent work of *Lundgren et al.* [2009], combining InSAR with geodetic data and models of the earthquake cycle to infer slip rates of 12 ± 9 mm/yr for each, the Coyote Creek and the Clark fault strands of the southern SJFZ.

[9] The ambiguity in the slip rate budget and initiation age for what might be the main plate boundary structure has implications for understanding the tectonic evolution of transform plate boundaries, and for kinematic fault models used to assess earthquake hazards in southern California. Kinematic models that attempt to explain temporal variability suggest a trade-off in slip rates between faults, implying that when one is fast the other is slow, thus the net rate should approach that of the plate boundary [*Sharp*, 1981; *Bennett et al.,* 2004]. Other kinematic fault models assume a constant slip rate along the entire length of a fault. However, mechanical models of faults show a systematic relationship between fault length and displacement with displacement decreasing towards the fault tip [*Cowie and Scholz,* 1992]. Thus, the range in slip rate estimates for the SJFZ could suggest that 1) the slip rate of the SJFZ may have decreased since its initiation, 2) faulting may have initiated earlier than 1.1 Ma [*Lutz et al.,* 2006; *Kirby et al.,* 2007], 3) a slip rate gradient may exist along the SJFZ, or 4) some

previously published slip rate estimates may have been compromised by insufficiently constrained ages or displacements.

3. METHODS

[10] Landforms along the Clark fault strand were mapped in the field using 1:5,000 and 1:10,000 scale contour maps constructed from high-resolution topography of the 'B4' Airborne Laser Swath Mapping [ALSM] experiment [*Bevis et al.,* 2005]. Following an initial reconnaissance survey, two sites (Rockhouse Canyon and the southern Santa Rosa Mountains) were chosen for a more detailed study, based on the following criteria: displaced landforms exhibited little post-depositional degradation, offsets were well defined, and suitable lithologies for ^{10}Be dating were present. At the northwestern site, in Rockhouse Canyon, the deflected modern channel (Channel 3) and two older beheaded channels (Channels 1 and 2) immediately SW of the fault were sampled for ^{10}Be dating. From each channel, we collected ~600 g samples from the top 1-3 cm of 7-9 quartz-bearing boulders. Samples collected from Channel 2 are from imbricated boulders lodged within relict bars that we interpret to have been deposited by debris flows. From Channel 1, due to the lack of preservation of imbricated deposits, five samples were collected from large, isolated boulders in the channel thalweg (samples Sjac 18-21 and 24) and four samples from boulders present on a relict alluvial fan terrace deposit ~1-2 m above the channel bottom (samples Sjac 14-17). To correct for inheritance, the top 2 cm of individual boulder tops from the thalweg of Channel 3 were collected ~100 m apart. At the southeastern site, in the southern Santa Rosa Mountains, we collected six ~500 g samples of quartz-bearing gravels and pebbles along a 2 m depth

profile within an offset alluvial fan deposit. The depth profile was collected from a recently incised natural cliff exposure after removing the outer ~0.2 m of sediment.

[11] The 250 to 500 μm size fraction of the crushed and sieved samples was chemically leached in the cosmogenic dating laboratories at the University of Cincinnati and Stanford University by a minimum of four acid leaches: one aqua regia leach; two high concentration (2-5%) HF/HNO_3 leaches; and one or more low concentration (1%) HF/HNO_3 leaches. To remove acid-resistant and mafic minerals, heavy liquid separations with lithium heteropolytungstate (LST, density 2.7 g/cm^3) were used after the first 5% HF/HNO_3 leach. Low background ^9Be carrier ($^{10}Be/^9Be$ ~1 x 10^{-15}) was added to the purified quartz, which was then dissolved in concentrated HF and fumed with perchloric acid. Fifteen to fifty grams of quartz was assumed for determining acid volumes used in the processing of chemical blanks. Next, the samples were passed through anion and cation exchange columns to separate the Be fractions. Ammonium hydroxide was added to the Be fractions to precipitate beryllium hydroxide gel. The beryllium hydroxide was oxidized by ignition in quartz crucibles at 750^{o}C to produce beryllium oxide. Beryllium oxide was then mixed with niobium powder and loaded in steel targets for the measurement of the $^{10}Be/^9Be$ ratios by accelerator mass spectrometry at the CAMS at the Lawrence Livermore National Laboratory or at the PRIME Laboratory at Purdue University.

[12] All ^{10}Be ages for sampled boulders were calculated using the CRONUS Age Calculator [*Balco et al.,* 2008; http://hess.ess.washington.edu/math/] (Table 2). No correction was made for geomagnetic field variations due to the ongoing debate regarding which, if any, correction factors are most appropriate. There also is considerable debate

regarding the use of appropriate scaling models [see *Balco et al.,* 2008] and we chose to use the time independent model of *Lal* [1991] and *Stone* [2000] to calculate our ages. However, we note that the different scaling models may produce age differences of up to 11%. Uncertainties associated with the age of each sample are presented in Table 2, these uncertainties include the internal (measured AMS uncertainty based on Poisson counting statistics) [*Gosse and Phillips,* 2001] and the 1 sigma external uncertainty (which is the total uncertainty associated with the method [*Gosse and Phillips*, 2001; *Balco et al*., 2008]).

[13] Landform exposure ages are affected by geologic factors, which include inheritance of ^{10}Be by prior exposure, toppling and exhumation of boulders, and weathering of boulders and alluvial fan surfaces. To estimate inheritance of ^{10}Be from hill slope residence and transport we collected 7 samples from boulders in the active channel 3. Not accounting for such inheritance would result in incorrectly old ages and lower slip rates. We assume that the sampled boulders have been exposed at least since the time that the channels were abandoned. Our field observations suggest little to no exhumation of boulders by winnowing of surrounding finer deposits. We also assume that the streams from a source area northeast of the Clark fault strand transported all the boulders that were sampled and that none of the sampled boulders originated from more recent collapse of hill slopes adjacent to the sample sites. To explore the potential effects of boulder weathering, we also calculated ^{10}Be exposure ages that account for 2m/Myr and 5m/Myr of surface attrition. These rates of erosion, if present, would result in modestly decreased slip rates as compared to the case of no boulder surface erosion.

4. RESULTS

4.1 ROCKHOUSE CANYON

[14] The Rockhouse Canyon site is located along the western range front of the Santa Rosa Mountains at the northernmost end of Clark Valley in the Anza Borrego desert (Fig. 2). At Rockhouse Canyon, strike-slip fault activity is mostly localized onto a single strand displaying channels in various stages of capture (Fig. 3). Two channels (Channel 1 and Channel 2) are completely beheaded from their source and no longer transporting large boulders (Fig. 3 and DR1). Contained within these channels are boulder bar deposits, fan deposits, and isolated boulders, which could only have originated from the present-day drainage areas located to the northeast of the fault (Fig. 3). Realignment of Channel 1 and Channel 2 indicates displacement of 500 ± 70 m and 220 ± 70 m, respectively (Fig. 3b). To realign the beheaded channels along the fault, we used contour maps derived from high-resolution topography to assess the maximum and minimum displacement from two drainage areas that could supply large boulders into the channel (Fig. 3B). The midpoint between the maximum and minimum distance is then used for the offset and the uncertainties associated with the displacement are based on the maximum and minimum distance permitted to realign the channels to their source (Fig. 3).

[15] To define the ages of these displacements, we determined ^{10}Be exposure ages of 8 to 9 boulders in each of the beheaded channels, and of 7 boulders in the active channel; the resulting 24 sample ages are presented in Table 2 and Figure 4. The error-weighted mean of the individual boulder ages from the active channel, 7.3 ± 3.0 ka, was used to infer the inheritance of ^{10}Be produced during exposure and transport prior to

boulder deposition in each channel. We note that this inheritance only defines prior exposure of ^{10}Be from the larger source area. The age of abandonment for each of the two beheaded channels is the error-weighted mean age of the individual boulder ages from the channel minus the 7.3 ± 3.0 ka inheritance age obtained from the active channel. This yields ages of 47 ± 8 ka for Channel 1, and 28 ± 9 ka for Channel 2 (age uncertainties given as the 95% confidence interval based on the 2-sigma external error associated with ^{10}Be model ages; Table 2). The age of one sample from Channel 1 (Sjac-17) was discarded because it is outside the 95% confidence interval of the average calculated from the remaining 8 exposure ages determined for this channel (Table 2; Figs. 4). The clustering of modeled ^{10}Be ages from individual boulders in each channel, combined with the dichotomy of ages between channels, gives us confidence that the boulders were likely transported and deposited in discrete subsequent episodes by one or both of the potential source streams (Table 2; Figs. 3 and 4).

[16] Fitting a single slip rate through both channel offsets versus their age yields an average late Quaternary to present slip rate of 8.9 ± 2.0 mm/yr for the Clark fault strand at Rockhouse Canyon. This rate is the error-weighted linear least squares fit of both the displacement and age, with uncertainty calculated at the 95% confidence interval. Because minor erosion of the boulder surface is permissible from field observations, we also calculated ages assuming 2 m/Myr and 5 m/Myr of boulder surface erosion, yielding lower slip rates of 7.8 ± 1.8 mm/yr, and 6.1 ± 1.4 mm/yr, respectively. Differencing the raw mean boulder ages (with no erosion) and displacements of Channel 1 from Channel 2 yields a significantly faster slip rate of 14.4 ± 3.4 mm/yr over the time interval from ~30-50 ka, followed by a slower rate of 7.7 ± 3.6 since ~30 ka. These two

slip rates from the same site could indicate temporal variation of the slip rate on the Clark fault strand over the latest Quaternary. However, at this time we cannot discriminate this apparent temporal variation from a constant slip rate with confidence.

4.2 SOUTHERN SANTA ROSA MOUNTAINS

[17] The southern Santa Rosa Mountains site of the Clark fault strand is located at the mouth of Rattlesnake Canyon on the southwestern range front of the Santa Rosa Mountains. Just to the southeast of this locality, the dextral Clark fault strand bends to the south into a set of normal-fault (horsetail) splays (Fig. 5). Alluvial fans emplaced across the Clark fault originate from the Santa Rosa Mountains plutonic and cataclastic zones, which are predominately comprised of tonalite, marble, and mylonitic gneiss [*Dibblee*, 1954; *Sharp*, 1967]. Using the nomenclature of *Bull* [1991] we map a Q2c alluvial fan surface that has been cut by dextral Clark fault slip. The alluvial fan surface at this site exhibits muted bar and swale microtopography, moderate desert pavement, and a slightly undulating surface morphology. Clasts on the surface display moderate to strong desert varnish development and strong rubification on their undersides. The Av soil horizon of the Q2c surface is ~1 cm thick and overlies a relic A horizon, that presumably formed before the Holocene, as the site is now in a hyper arid soil moisture regime. These observations imply that there has been minimal denudation and aggradation of the surface during the extremely arid local climate of the past 8-12 ka.

[18] The fan surface is cut by multiple fault strands, but only one of these shows significant dextral offset. The displacement along this strand is estimated as 51 ± 9 m (Fig. 5 and DR1), using a beheaded channel (Channel 1) and two deflected channels

(Channels 1 and 2) as piercing lines (Fig. 5). To reconstruct this offset, we used contour maps derived from high-resolution topography and field measurements to assess the maximum and minimum distance that would permit all three channels to align. We note that Channel 3 has two potential upstream piercing lines northeast of the fault (Fig. 5). However, we choose to realign Channel 3 with the more eastern drainage area and not the midpoint of the two northeast sources because in doing so will cause mis-alignment of channels 2 and 3. The uncertainty associated with the offset is based on the maximum and minimum distance permitted to realign all three channels. This distance is minimized by lining up the thalweg and wall (9 m width) of beheaded Channel 1 on both sides of the fault (Fig. 5).

[19] To determine the slip rate, we dated the fan surface using ^{10}Be concentrations from a 2 m-deep vertical stream-cut exposure. The age was determined from the slope of a linear least-squares fit of ^{10}Be concentration versus exp(-z/z*), where z is depth and z* is the depth where ^{10}Be production declines by 1/e (Fig. 6). The intercept of this line with zero (i.e., infinite depth) yields an estimate of the ^{10}Be inheritance of the sediment. This implies a ^{10}Be depth profile age of 35 ± 7 ka (95% confidence) for the displaced fan surface, yielding a slip rate of 1.5 ± 0.4 mm/yr (Table 2 and Fig. 6). The uncertainty associated with the slip rate is the root mean squared error for both age and offset. Although a robust method to deduce the ^{10}Be surface concentration [*Anderson et al.*, 1996; *Repka et al.*, 1997], ages determined from the depth profile may be subject to erosion that will reduce the apparent surface age. However, soil characteristics from the displaced Q2c surface imply that minimal surface lowering has occurred since 8-12 ka,

giving us confidence that our modeled age is reliable and has not been modified by major surface lowering, at least during the Holocene.

6. DISCUSSION

[20] Our new data allow us to compare slip rate estimates over the same time interval (the past 30-50 ka) along the Clark fault strand of the SJFZ from Anza to the southern Santa Rosa Mountains. Since ~30-50 ka, our results show a pronounced southward slip rate decrease along the Clark fault strand. The ~13 mm/yr late Quaternary rate at Anza [*Rockwell et al.,* 1990] decreases southeastward to 8.9 ± 2.0 mm/yr at Rockhouse Canyon and to 1.5 ± 0.4 mm/yr at the southern Santa Rosa Mountains (Fig. 2). This southward gradient in slip rate along the Clark fault strand is consistent with a similar decrease in slip per event for the past several events, as documented from small channel offsets [*Middleton*, 2006; *Bull*, *personal communication*, 2008]. This decrease is also consistent with the decrease in total bedrock displacement [*Sharp*, 1967] from Anza (22-24 km) to Rockhouse Canyon (~14.5 km) (Fig. 2). Farther southeast, toward the southern Santa Rosa Mountains, the total bedrock displacement has been estimated to be similar to that at Rockhouse Canyon (~14.5 km) [*Sharp*, 1967], but because the offset cataclasite marker is as much as 5 km away from the main fault strand (Fig. 2) this estimate is less well constrained. The consistent decrease in total bedrock offset and slip rate between Anza and Rockhouse Canyon can be attributed to a transfer of slip onto the adjacent Coyote Creek fault strand (Fig. 2) [*Sharp,* 1967]. A plausible explanation for the more dramatic decrease in slip rate from Rockhouse Canyon to the Santa Rosa Mountains is that much of the deformation has been absorbed by young and active distributed

deformation in the Borrego Badlands basin, where slip has juxtaposed thick sediments of the Salton Trough against bedrock of the Santa Rosa Mountains (Fig. 2) [*Belgarde and Janecke,* 2007], and some displacement may also be taken up by the Coyote Mountain and Inspiration Point faults (Fig.2). Overall, the Clark fault strand exemplifies how slip rates are not maintained along the entire length of faults and that considerable strain may be accommodated in a distributed manner, especially near the fault tip [*Cowie and Scholz,* 1992]. Gradients in slip rate appear to be especially dramatic where faulting juxtaposes sedimentary rocks [*Cowie and Scholz,* 1992].

[21] The strong correlation between total bedrock displacement and our late Quaternary slip rates along the Clark fault strand between Anza and Rockhouse Canyon leads to interesting speculations on fault system behavior. Assuming that fault slip rates have been constant since fault inception, our rates are slower than required by the ca. ~1.1 Ma inception of dextral faulting proposed for the Salton Trough by *Lutz et al.* [2006] and *Kirby et al.* [2007]. Conversely, if we combine bedrock displacements and slip rates at Anza (22-24 km and ~12-15 mm/yr, respectively) and Rockhouse Canyon (14.5 km and 8.9 ± 2.0 mm/yr, respectively), we would estimate the age of fault initiation at both sites as 1.7 ± 0.3 Ma. This earlier onset, which is consistent with constraints from the San Timoteo badlands [*Matti and Morton,* 1993] could also be permitted in the Salton Trough if some slip on the Clark fault accrued prior to the dramatic stratigraphic transition documented by *Lutz et al.,* [2006] and *Kirby et al.,* [2007]. A 1.7 ± 0.3 Ma initiation age of the SJFZ is also consistent with thermochronologic studies from the San Bernardino Mountains at Yucaipa Ridge, which are thought to have uplifted contemporaneously with initiation of the SJFZ [*Morton and Matti,* 1993, *Spotila et al.,*

2001] and show rapid exhumation since ~1.8 Ma (U-Th/He apatite age) [*Spotila et al.*, 2001]. Alternatively, slip rates at both Anza and Rockhouse Canyon may have decreased together in the late Quaternary. This would suggest that the mechanism responsible for the trade-off in slip from the Clark fault strand to the Coyote Creek fault strand acts independently of the rate of strain accumulation across the entire southern SJFZ.

[22] The slip rate estimates presented in this study support a consistent overall rate of strain accumulation across the southern SJFZ of 10 to 14 mm/yr over the late Quaternary. Taking our late Quaternary rate from Rockhouse Canyon (8.9 ± 2.0 mm/yr) as representative of the current slip rate of the southern Clark fault strand, and combining this with previously published Holocene slip rates for the Coyote Creek fault strand [~1-5 mm/yr: *Clark et al.,* 1972; *Sharp,* 1981; *Pollard and Rockwell*, 1995], suggests that the southern SJFZ accommodates ~10 to 14 mm/yr of plate boundary motion. This rate is similar to the combined slip rates of the Superstition Mountain fault [5-9 mm/yr: *Gurrola and Rockwell,* 1996] and Superstition Hills fault [3-6 mm/yr: *Hudnut and Sieh,* 1989] as well as the slip rate near Anza where the Clark fault is essentially the single strand of the SJFZ [*Rockwell et al.*, 1990; *Rockwell,* 2008]. Combining slip rates across a transect from the southern Santa Rosa Mountains locality (1.5 ± 0.4 mm/yr) with previously determined Holocene slip rates for the Coyote Creek fault (~1-5 mm/yr) implies a southward slip rate decrease across the southern SJFZ, from ~10-14 mm/yr in its central portion to ~2-7 mm/yr near the fault at the latitude of the Borrego and Fish Creek badlands (Figs. 1 and 2); however, the residual strain in this region is presumably accommodated through folding and thrusting in the adjacent Borrego Badlands basin [*Belgarde and Janecke,* 2006]. Farther south, the entire 8-15 mm/yr may be

accommodated by slip along the Superstition Hills and Superstition Mountain faults (*Gurrola and Rockwell,* 1996, *Hudnut and Sieh,* 1989), at least in the Holocene. Comparing these results with the 15.9 ± 3.4 mm/yr slip rate determined over the same late Quaternary time interval for the Indio segment of the San Andreas fault [*van der Woerd et al.,* 2006] suggests that the SJFZ is probably subordinate to the southern San Andreas fault zone, although it is also possible (within uncertainties) that deformation is partitioned fairly evenly between the two. The remaining plate boundary strain in this region is likely taken up by the Elsinore fault, the Eastern California Shear Zone, NE-striking cross-faulting, and locally distributed folding and thrusting.

[23] Our slip rate estimates for the Clark fault strand show pronounced spatial variability, and possible temporal variability of fault slip rates along the southern San Andreas fault system during the late Quaternary. This, in turn, suggests a complex kinematic evolution, which may explain apparent discrepancies between slip rate estimates obtained from geologic and geodetic data. Our results are at odds with combined InSAR and GPS data, which suggest much higher slip rates for the southern SJFZ [*Fialko,* 2006; *Lundgren et al.,* 2009], but consistent with GPS block models, as well as elastic and viscoelastic models of crustal deformation in this region [*Bennett et al.,* 1996; *Meade and Hager,* 2005; *Becker et al.,* 2005; *Fay and Humphreys,* 2005]; the large differences of these geodetically derived slip rates may result from differences in modeling approaches, or temporal and spatial coverage of the geodetic data. Seismic hazard studies commonly rely on long-term Quaternary rates to infer short-term hazard. Our observations suggest that information at many different localities along a fault and

over multiple time frames is needed to adequately construct kinematic models and to better assess earthquake hazards along evolving plate margins.

7. CONCLUSION

[24] The Clark fault strand of the southern SJFZ displays a pronounced southeastward decrease in late Quaternary slip rate. ^{10}Be exposure ages of 47 ± 8 ka and 28 ± 9 ka for two beheaded channels and 35 ± 7 ka for a displaced alluvial deposit imply slip rates of 8.9 ± 2.0 mm/yr at Rockhouse Canyon and 1.5 ± 0.4 mm/yr for the southern Santa Rosa Mountains. This gradient in slip rate must be largely accommodated by distributed deformation within the Salton Trough and the transfer of slip to the Coyote Creek fault. Our results show that, at least for the past ~30-50 kyr, the SJFZ may have been equivalent, but more likely was subordinate, to the southern San Andreas fault in accommodating plate margin strain. This suggests that either the slip rate of the San Jacinto fault has decreased since its initiation or faulting began earlier than 1.1 Ma.

ACKNOWLEDGEMENTS

This research was supported by the Southern California Earthquake Center (SCEC). SCEC is funded by NSF Cooperative Agreement EAR-0529922 and USGS Cooperative Agreement 07HQAG0008. The SCEC contribution number for this paper is 1295. This research was also supported by NEHRP grant G00006871. Special thanks to Alana Wilson and Eitan Shelef for field assistance, George Hilley for use of the cosmogenic nuclide extraction laboratory at Stanford University, George Jefferson and all the Rangers

and volunteers (especially the Shuguns and Keeleys) at the Anza Borrego State Park for their help throughout the field work and the 2008 FOP participants for their lively discussions and comments. We also thank Robert Finkel and Dylan Rood for AMS measurements at the Lawrence Livermore National Laboratory. We would also like to express our sincere thanks to Richard Lease and an anonymous reviewer and editor who provided insightful and constructive comments on our manuscript.

Figure 1. Location map showing the study area along the southern San Jacinto fault zone. Inset shows the index map for major faults in southern California. References: (a) *Clark et al*. [1972], *Sharp* [1981], *Pollard and Rockwell* [1995]; (b) *Hudnut and Sieh* [1989]; and (c) *Gurrola and Rockwell* [1996].

Figure 2. Geologic map of the southern San Jacinto fault zone. The black arrows show the amount of displacement of plutonic, metamorphic and cataclastic rocks mapped by *Sharp* [1967]. The white star indicates the location of a previous study along the Clark fault at Anza [Rockwell et al., 1990]. The white stars with a black dot indicate the locations where we determined the slip rates reported in the present study.

Figure 3. [A] ALSM image of the Rockhouse Canyon site. Frame shows the location of [B]. [B] Location of beheaded and deflected channels at Rockhouse Canyon; the left panel is the present-day configuration of Channels 1, 2 and 3; the center panel is the

reconstruction for Channel 2; the right panel is the reconstruction for Channel 1. The black solid lines indicate the maximum and minimum displacements from the source drainage(s) for offset channels. The dots in panel [B] indicate the location of boulder samples collected for ^{10}Be exposure dating. See Fig. 2 for location.

Figure 4. Chart showing the error-weighted mean age of Channel 1, Channel 2 and Channel 3. ^{10}Be surface exposure ages of boulders from Channel 1 and Channel 2 do not include inheritance from Channel 3. The gray and black vertical bars are ages of individual boulder samples used in calculating the age of each channel. The inset-shaded box within each vertical bar is the ^{10}Be model age and associated internal uncertainity with the AMS measurement. The white vertical bar is an outlier that is outside the 95% confidence interval of the remaining 8 samples from Channel 1. Please see text and Table 2 for details.

Figure 5. ALSM image of the southern Santa Rosa Mountains site. [A] The present-day configuration of 3 channels incised into the Q2c surface. Inset: fault map showing traces of the Clark fault in [A]; [B, C] The present-day configuration of beheaded and deflected channels incised into the Q2c fan deposit. The white star in [C] is the location of the 2 m deep depth profile sampled for ^{10}Be surface exposure age dating. [D] The reconstruction of a beheaded channel (Channel 1) and two deflected (Channels 2 and 3) for 35 ± 7 kyr ago. Please see text and Table 2 for details.

Figure 6. Field photo and graph of the exponential decrease in the concentration of ^{10}Be with depth from an alluvial surface cut by the Clark fault at the southern Santa Rosa Mountain locality. The stippled black lines indicate the 95% confidence interval around the black regression line. Vertical dotted lines represent the inheritance and its associated errors. The regression line indicates a surface age of 35 ± 7 ka.

References:

Anderson, R. S., J. L. Repka, and G. S. Dick (1996), Explicit treatment of inheritance in dating depositional surfaces using in situ 10Be and 26Al, *Geology, 24*, 47-51. 10.1130/0091-7613(1996)024.

Balco, G., J. O. Stone, N. A. Lifton, and T. J. Dunai (2008), A complete and easily accessible means of calculating surface exposure ages or erosion rates from 10Be and 26Al measurements, *J. Quat. Geochron., 3*, 174-195. 10.1016/j.quageo.2007.12.001.

Becker, T., J. Hardebeck, and G. Anderson (2005), Constraints on fault slip rates of the southern California plate boundary from GPS velocity and stress inversions, *Geophy. J. Int., 160*, 634-650. 10.1111/j.1365-246X.2004.02528.

Belgarde, E., and S. U. Janecke (2006), Structural characterization and microseismicity near the SE end of the Clark fault of the San Jacinto fault in the southwestern Salton Trough, *Abstracts*

for the SCEC Annual Meetings.

Bennett, R., A. Friedrich, and K. Furlong (2004), Codependent histories of the San Andreas and San Jacinto fault zones from inversion of fault displacement rates, *Geology*, *32*, 961-965. 10.1130/G20806.1.

Bennett, R. A., W. Rodi, and R. E. Reilinger (1996), Global Positioning System constraints on fault slip rates in southern California and northern Baja, Mexico, *J. Geophys. Res., 101*, 21, 943-921. 10.1029/96JB02488.

Bevis, M., K. Hudnut, R. Sanchez, C. Toth, D. Grejner-Brzezinska, E. Kendrick, D. Caccamise, D. Raleigh, H. Zhou, h. H. Z. S. Shan, W. Shindle, A. Yong, J. Harvey, A. Borsa, F. Shrestha, B. Carter, M. Sartori, D. Phillips, and F. Coloma (2005), The B4 Project: Scanning the San Andreas and San Jacinto Fault Zones, *Eos Trans. AGU, American Geophyiscal Union, Fall Meeting*, #H34B-01.

Bull, W. B. (1991), Geomorphic responses to climatic change, *Oxford Univeristy Press: New York.*

Clark, M. M. (1972), Surface Rupture Along the Coyote Creek Fault, *USGS Professional Papers*, *787*, 55-86.

Cowie, P. A., and C. H. Scholz (1992), Physical explanation for the displacement-length

relationship of faults using a post-yield fracture mechanics model, *J. Struc. Geol.*, *14*, 1133-1148.

DeMets, C., and T. H. Dixon (1999), New kinematic models for Pacific-North America motion from 3 Ma to present, I: Evidence for steady state motion and biases in the NUVEL-1A model, *Geophy. Res. Lett.*, *26*, 1921-1924. 10.1029/1999GL900405.

Dibblee, T. W. (1954), Geology of the Imperial Valley region, California, *in Jahns, R.H., ed., Geology of southern California*, California Division of Mines Bulletin 170.

Dorsey, R. J. (2002), Stratigraphic record of Pleistocene initiation and slip on the Coyote Creek fault, lower Coyote Creek, southern California, *Contributions to crustal evolution of the Southwestern United States, Geol. Soc. Am. Spec. Publ. 365*, 251-269.

Fay, N., and G, Humphreys (2005), Fault slip rates, effects of elastic heterogeneity on geodetic data, and the strength of the lower crust in the Salton Trough region, southern California, *J. Geophys. Res.*, *110*, 1-14. 10.1029/2004JB003548.

Fialko, Y. (2006), Interseismic strain accumulation and the earthquake potential on the southern San Andreas fault system, *Nature*, *441*, 968-971. 10.1038/nature04797.

Gosse, J.C. and F.M. Phillips, (2001), Terrestrial in-situ cosmogenic nuclides: theory and applications, *Quat. Sci. Rev, 20*, 1475-1560

Gurrola, L. D., and T. K. Rockwell (1996), Timing and slip for prehistoric earthquakes on the Superstition Mountain fault, Imperial Valley, southern California, *J. Geophys. Res., 101*, 5977-5985. 10.1029/95JB03061

Harden, J. W., and J. C. Matti (1989), Holocene and late Pleistocene slip rates on the San Andreas fault in Yucaipa, California, using displaced alluvial-fan deposits and soil chronology, *Geol. Soc. Am. Bull., 101*, 1107-1117. 0.1130/0016-7606(1989)101.

Hudnut, K., and K. Sieh (1989), Behavior of the Superstition Hills fault during the past 330 years, *Bull. Seis. Soc. Am., 79*, 304-329.

Janecke, S.U., R.J. Dorsey, A.N. Steely, S.M. Kirby, A. Lutz, B.A. Housen, B. Belgarde, V. Langenheim, T. Rittenour, and D. Forand, (2008) High Geologic Slip Rates since Early Pleistocene initiation of the San Jacinto and San Felipe Fault Zones in the San Andreas fault system: Southern California, USA. *Abstracts for the SCEC Annual Meetings.*

Johnson, H. O., D. C. Agnew, and F. K. Wyatt (1994), Present-day crustal deformation in southern California, *J. Geophys. Res., 99*, 23,951-923,974. 10.1029/94JB01902.

Kendrick, K. J., D. M. Morton, S. G. Wells, and R. W. Simpson (2002), Spatial and temporal deformation along the northern San Jacinto fault, southern California: Implications for slip rates, *Bull. Seis. Soc. Am., 92*, 2782-2802. 10.1785-/0120000615.

King, N. E., and J. C. Savage (1983), Strain-rate profile across the Elsinore, San Jacinto, and San Andreas faults near Palm Springs, California, 1973-1981, *Geophy. Res. Lett.*, *10*, 55-57. 10.1029/GL010i001p00055.

Kirby, S. M., S. U. Janecke, and R. J. Dorsey (2007), Pleistocene Brawley and Ocotillo Formations: Evidence for initial strike-slip deformation along the San Felipe and San Jacinto fault zones, southern California, *Jour. Geol.*, *115*, 43-62. 10.1086/509248.

Lal, D. (1991), Cosmic ray labeling of erosion surfaces-In situ nuclide production rates and erosion models, *Earth Planet. Sci. Lett.*, *104*, 424-439. 10.1016/0012-821X(91)90220-C.

Lundgren, P., E. A. Hetland, Z. Liu, and E. J. Fielding (2009), Southern San Andreas-San Jacinto fault system slip rates estimated from earthquake cycle models constrained by GPS and Interferometric synthetic aperture radar observations, *J. Geophys. Res.*, *114*, B02403. 10.1029/2008JB005996.

Lutz, A. T., R. J. Dorsey, B. A. Housen, and S. U. Janecke (2006), Stratigraphic record of Pleistocene faulting and basin evolution in the Borrego Badlands, San Jacinto fault, southern California, *Geol. Soc. Am. Bull.*, *118*, 1377-1397. 10.1130/B25946.1.

Matmon, A., D. Schwartz, R. Finkel, S. Clemmens, and T. Hanks (2005), Dating offset fans along the Mojave section of the San Andreas fault using cosmogenic 26Al and 10Be, *Geol. Soc.*

Am. Bull., *117*, 795-807. 10.1130/B25590.1.

Meade, B. J., and B. H. Hager (2005), Block models of crustal motion in southern California constrained by GPS measurements, *J. Geophys. Res.*, *110*, B03403. 10.1029/2004JB003209.

Middleton, T. (2006), Tectonic Geomorphology of the Southern Clark Fault from Anza Southeast to the San Felipe Hills: Implications of Slip Distribution for Recent Past Earthquakes, *Master's Thesis., San Diego State University*, 95 p.

Morton, D. M., and J. C. Matti (1993), Extension and contraction within an evolving divergent strike-slip fault complex: the San Jacinto fault zones at their convergence in Southern California, *The San Andreas fault system: displacement, Geol. Soc. Am. Mem. 178*, 107-159.

Oskin, M. E., K. Le, and M. D. Strane (2007), Quantifying fault-zone activity in arid environments with high-resolution topography, *Geophy. Res. Lett.*, *34*, L23SO25.10.1029/2007GL031295.

Pollard, W., and T. Rockwell (1995), Late Holocene slip rate for the Coyote Creek fault, Imperial County, California, *Abstract Geol. Soc. Am. Meeting*, *27*, p. 72.

Repka, J. L., R. S. Anderson, and R. Finkel (1997), Cosmogenic dating of fluvial terraces, Fremont River, Utah, *Earth Planet. Sci. Lett.*, *152*, 59-73. 10.1016/S0012-821X(97)00149-0.

Richards-Dinger, K. B., and P. M. Shearer (2000), Earthquake locations in southern California obtained using source-specific station terms, *J. Geophys. Res., 105*, 10, 939-10,960. 10.1029/2000JB9000014.

Rockwell, T. K. (2008), Observations of Mode-Switching From Long Paleoseismic Records of Earthquakes on the San Jacinto and San Andreas Faults: Implications for Making Hazard Estimates From Short Paleoseismic Records, *Intern. Geol. Congr. Meeting: Oslo, Norway.*

Rockwell, T. K., C. Loughman, and P. Merifield (1990), Late Quaternary rate of slip along the San Jacinto fault zone near Anza, southern California, *J. Geophys. Res., 95*, 8593-8605. 10.1029/JB095iB06p08593.

Rockwell, T. K., G. Seitz, T. Dawson, and J. Young (2006), The long record of San Jacinto fault paleoearthquakes at Hog Lake: Implications for regional patterns of strain release in the southern San Andreas fault system, *Seis. Res. Lett.*, *77*, 270.

Sharp, R. V. (1967), San Jacinto fault zone in the Peninsular Ranges of southern California, *Geol. Soc. Am. Bull.*, *78*, 705-730. 10.1130/0016-7606(1967)78.

Sharp, R. V. (1981), Variable rates of late Quaternary strike slip on the San Jacinto fault zone, southern California, *J. Geophys. Res.*, *86*, 1754-1762. 10.1029/JB086iB03p01754.

Spotila, J. A., K. A. Farley, J. D. Yule, and P. W. Reiners (2001), Near-field transpressive

deformation along the San Andreas fault zone in southern California, based exhumation constrained by (U-Th)/He dating, *J. Geophys. Res., 106*, 30, 909-930, 10.1029/2001JB000348.

Stone, J. O. (2000), Air pressure and cosmogenic isotope production, *J. Geophys. Res.*, *105*, 23,753-723,759. 10.1029/2000JB90081.

Thatcher, W., J. A. Hileman, and T. Hanks (1975), Seismic slip distribution along the San Jacinto fault zone, southern California, and its implications, *Geol. Soc. Am. Bull.*, *86*, 1140-1146. 10.1130/0016-7606(1975)86.

van der Woerd, J., Y. Klinger, and K. Sieh (2006), Long-term slip rate of the southern San Andreas Fault from 10Be-26Al surface exposure dating of an offset alluvial fan, *J. Geophys. Res., 111*, B04407. 10.1029/2004JB003559.

Weldon, R. J., and K. E. Sieh (1985), Holocene rate of slip and tentative recurrence interval for large earthquakes on the San Andreas fault, Cajon Pass, southern California, *Geol. Soc. Am. Bull., 96*, 793-812. 10.1130/0016-7606(1985)96.

Wesnousky, S. G., C. S. Prentice, and K. Sieh (1991), An offset Holocene stream channel and the rate of slip along the northern reach of the San Jacinto fault zone, San Bernardino Valley, *Geol. Soc. Am. Bull., 103*, 700-709. 0.1130/0016-7606(1991)103.

Table 1. Published slip rates for the San Jacinto fault zone

Time Frame	Reference	Slip Rate	Notes
Geodetic	*Bennett et al.* [1996]	9 ± 2 mm/yr	GPS & elastic block model of crustal deformation
	Bennett et al. [2004]	8 ± 4 mm/yr	Codependent slip history model from published slip rates
	Becker et al. [2005]	15 ± 1 mm/yr	GPS & stress-field orientations from earthquake focal mechanisms
	Meade and Hager [2005]	12 ± 1 mm/yr	GPS & block model of crustal deformation
	Fay and Humphreys [2005]	15 ± 1 mm/yr	GPS & block model of crustal deformation
	Fialko [2006]	21 ± 1 mm/yr	InSAR & GPS
	Lundgren et al. [2009]	12 ± 9 mm/yr (Clark strand) 12 ± 9 mm/yr (Coyote Creek strand)	InSAR, GPS & earthquake cylcle
Latest Holocene	*Sharp* [1981]	2 ± 1 mm/yr (Coyote Creek strand)	Offset of AD 1650 shoreline of Lake Cahuilla
	Wesnousky et al. [1991]	>1.7-3.3 mm/yr	Offset channel margin and C-14 dating
	Rockwell [2008] *Rockwell et al.* [2006}	12-15 mm/yr	Includes 5-event cluster of activity from AD 1025 to AD 1360.
Late Quaternary	*Rockwell et al.* [1990]	> 9 ± 2 mm/yr	Minimum offset along shutter ridge since 9.5 ka from C-14
		$11\ ^{+9}/_{-5}$ mm/yr	Channel inset into Q3b (~14 ka-soil age) terrace offset 150 ± 30 m
		$12\ ^{+9}/_{-5}$ mm/yr	Channel inset into Q4 (~17 ka-soil age) terrace offset 210 ± 20 m
		$13\ ^{+10}/_{-6}$ mm/yr	Channel inset into Q5 (~50 ka-soil age) terrace offset 620 ± 40 m
	Kendrick et al. [2002]	~20 mm/yr	Dextral slip rate estimated from elastic model of uplift rates along restraining fault geometry.
Mid-Quaternary	*Sharp* [1981]	10 ± 2 mm/yr	5.7 to 8.6 km offset alluvial fan deposit overlying 760 ka Bishop Ash at Anza
	Morton and Matti [1993]	16 mm/yr	Inception of faulting at 1.5 Ma and 23 ± 1 km displacement from Sharp (1967)
	Dorsey [2002]	10 ± 3 mm/yr (Coyote Creek strand)	Inception of faulting at 600 ka and 6 km approximate displacement

Table 2. SUMMARY OF SAN JACINTO FAULT ^{10}Be MODEL AGES

Sample name	Thickness (cm)	Shielding correction	Altitude (m)	Latitude (DD)	Longitude (DD)	^{10}Be measured (10^6 atom g^{-1})	^{10}Be age (ka) 0m/Myr	Error# ± (ka)	Error* ± (ka)	^{10}Be age (ka) 2m/Myr	Error* ± (ka)	^{10}Be age (ka) 5m/Myr	Error* ± (ka)
Channel 1													
Sjac-14	1	1.000	561	33.4052	-116.3708	0.4352 ± 0.0155	63.7	2.3	6.1	71.5	7.7	90.2	13.0
Sjac-15	3	1.000	561	33.4052	-116.3707	0.4734 ± 0.0163	70.6	2.5	6.7	80.3	8.8	105.4	16.3
Sjac-16	4	1.000	560	33.4051	-116.3707	0.3521 ± 0.0363	52.7	5.5	7.2	57.9	8.7	69.1	12.8
Sjac-17†	2	1.000	563	33.4054	-116.3708	0.5900 ± 0.0346	87.5	5.2	9.3	103.2	13.3	153.9	34.5
Sjac-18	2	1.000	564	33.4056	-116.3709	0.4002 ± 0.0137	58.9	2.0	5.6	65.5	6.9	80.4	11.0
Sjac-19	4	1.000	566	33.4058	-116.3709	0.3735 ± 0.0268	55.7	4.0	6.4	61.6	7.8	74.5	11.9
Sjac-20	2	1.000	572	33.4061	-116.3710	0.2727 ± 0.0406	39.7	6.0	6.9	42.6	8.0	48.0	10.3
Sjac-21	5	1.000	589	33.4066	-116.3712	0.3130 ± 0.0143	46.2	2.1	4.6	50.1	5.4	58.0	7.4
Sjac-24	5	1.000	614	33.4076	-116.3710	0.3639 ± 0.0106	52.8	1.6	4.9	58.0	5.9	69.1	8.7
Weighted mean of sample ages ± error**							**54.4 ± 7.5**			**59.4 ± 8.9**		**69.1 ± 10.4**	
Inheritance corrected sample ages ± error**							**47.3 ± 7.7**			**52.3 ± 9.3**		**62.1 ± 13.0**	
Channel 2													
Sjac-33	3	0.977	587	33.4061	-116.3657	0.3169 ± 0.0222	47.6	3.4	5.4	51.8	6.4	60.3	8.9
Sjac-34	3	0.979	577	33.4053	-116.3656	0.1930 ± 0.0048	29.0	0.7	2.6	30.5	2.9	33.1	3.5
Sjac-35	4	0.985	573	33.4046	-116.3644	0.2523 ± 0.0059	38.2	0.9	3.5	40.9	4.0	45.9	5.1
Sjac-36	3	0.988	567	33.4039	-116.3640	0.3433 ± 0.0078	51.8	1.2	4.7	56.8	5.7	67.5	8.3
Sjac-37	3	0.989	561	33.4033	-116.3635	0.2884 ± 0.0052	43.5	0.8	3.9	46.9	4.6	53.7	6.1

Sjac-38	5	0.975	545	33.4025	-116.3631	0.2867 ± 0.0067	45.3	1.1	4.1	49.0	4.8	56.5	6.6
Sjac-39	2	0.976	546	33.4017	-116.3630	0.1871 ± 0.0049	28.7	0.8	2.6	30.1	2.9	32.7	3.4
Sjac-40	2	0.977	527	33.4039	-116.3664	0.1435 ± 0.0039	22.3	0.6	2.0	23.1	2.2	24.6	2.5
Weighted mean of sample ages ± error**							**32.3 ± 8.5**			**36.6 ± 9.5**		**41.1 ± 10.7**	
Inheritance corrected sample ages ± error**							**27.8 ± 8.8**			**29.3 ± 9.9**		**31.4 ± 11.9**	
Channel 3													
Sjac-25	4	1.000	587	33.4067	-116.3681	0.0333 ± 0.0039	4.9	0.6	1.3				
Sjac-27	3	1.000	577	33.4063	-116.3680	0.0715 ± 0.0044	10.5	0.6	1.8				
Sjac-28	3	1.000	573	33.4060	-116.3679	0.0370 ± 0.0049	5.5	0.7	1.6				
Sjac-29	3	1.000	567	33.4055	-116.3675	0.0893 ± 0.0055	13.6	0.8	2.3				
Sjac-30	4	1.000	561	33.4055	-116.3675	0.0486 ± 0.0038	7.5	0.6	1.5				
Sjac-31	4	1.000	545	33.4046	-116.3666	0.0991 ± 0.0067	15.6	1.1	2.8				
Sjac-32	1	1.000	546	33.4048	-116.3667	0.0397 ± 0.0036	6.2	0.6	1.3				
Weighted mean of sample ages ± error**							**7.3 ± 3.0**						

	Depth (cm)					
SJF-P1	0	1.000	314	33.2967	-116.1677	0.2437 ± 0.0104
SJF-P2	20	1.000	314	33.2967	-116.1677	0.1967 ± 0.0080
SJF-P3	50	1.000	314	33.2967	-116.1677	0.1456 ± 0.0030
SJF-P4	83	1.000	314	33.2967	-116.1677	0.1272 ± 0.0029

SJF-P5	136	1.000	314	33.2967	-116.1677	0.1006 ± 0.0020
SJF-P6	175	1.000	314	33.2967	-116.1677	0.0667 ± 0.0001
Model age ± error						**34.5 ± 6.6**

Notes: ^{10}Be model ages calculated using the CRONUS calculator at Rockhouse Canyon (see Figs. 2,3 and 6 for sample locations).

Abbreviations: DD is decimal degrees.

#Internal error associated with AMS measurement.

*External error associated with ^{10}Be model exposure ages.

**95% confidence interval of the 2-sigma external error associated with ^{10}Be model exposure ages.

†Boulder samples that are not used in the calculation of the weighted mean age. See text for details.

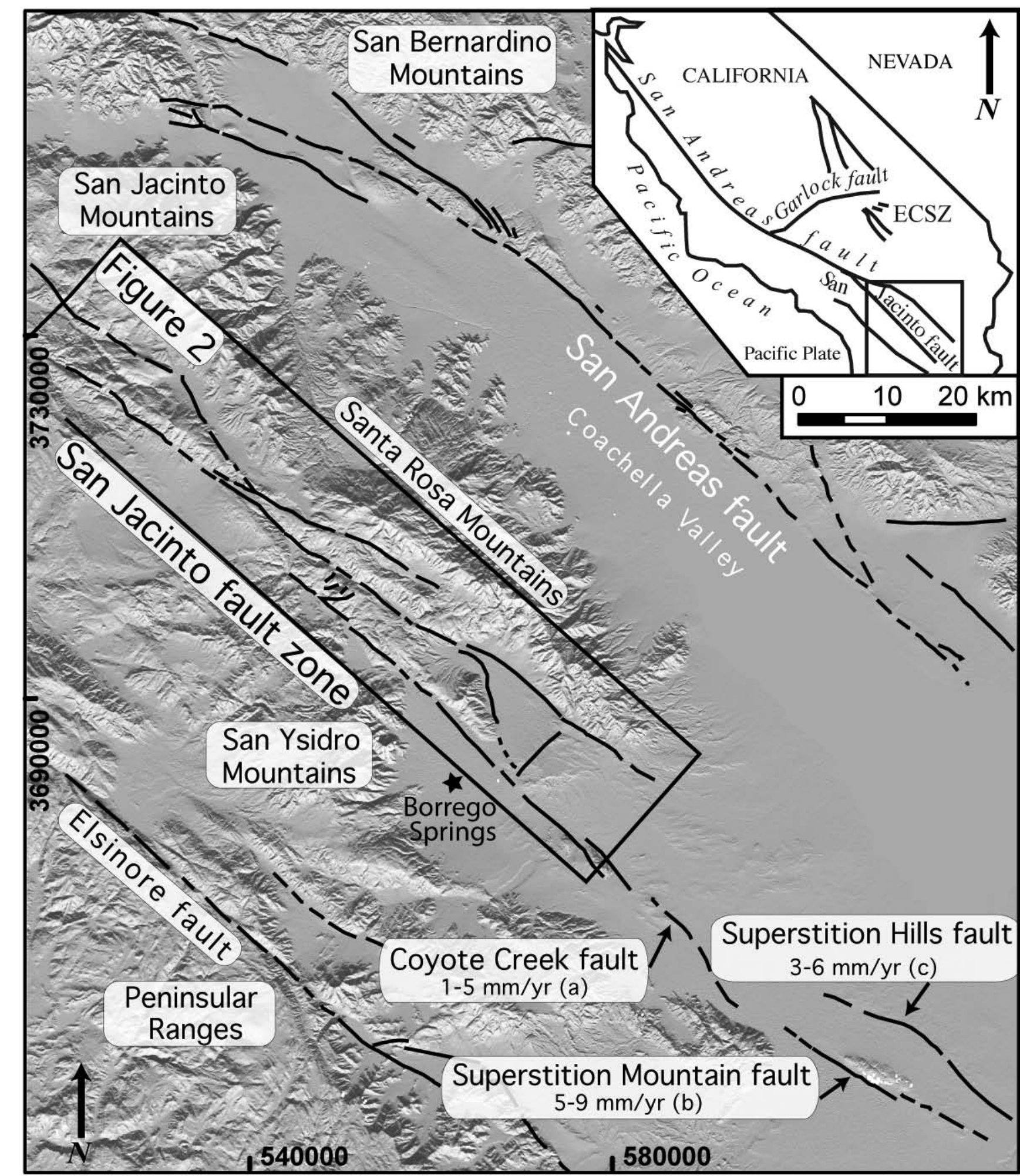
San Bernardino Mountains
San Jacinto Mountains
Figure 2
San Jacinto fault zone
Santa Rosa Mountains
San Andreas fault
Coachella Valley
San Ysidro Mountains
Borrego Springs
Elsinore fault
Peninsular Ranges
Coyote Creek fault
1-5 mm/yr (a)
Superstition Hills fault
3-6 mm/yr (c)
Superstition Mountain fault
5-9 mm/yr (b)
3730000
3690000
540000
580000
N
CALIFORNIA
NEVADA
San Andreas fault
Garlock fault
ECSZ
Pacific Ocean
San Jacinto fault
Pacific Plate
0 10 20 km

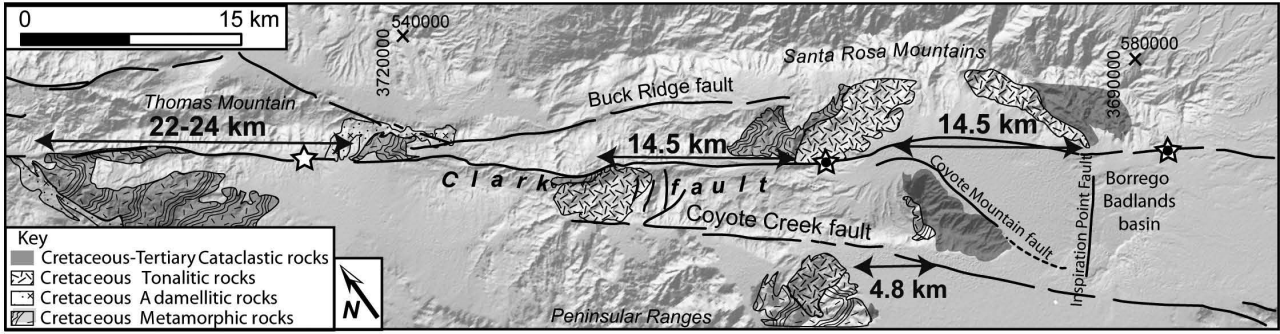
0
15 km
540000
3720000
580000
3690000
Santa Rosa Mountains
Thomas Mountain
22-24 km
Buck Ridge fault
14.5 km
14.5 km
Clark fault
Coyote Creek fault
Coyote Mountain fault
Inspiration Point Fault
Borrego Badlands basin
4.8 km
Peninsular Ranges
Key
Cretaceous-Tertiary Cataclastic rocks
Cretaceous Tonalitic rocks
Cretaceous A damellitic rocks
Cretaceous Metamorphic rocks
N

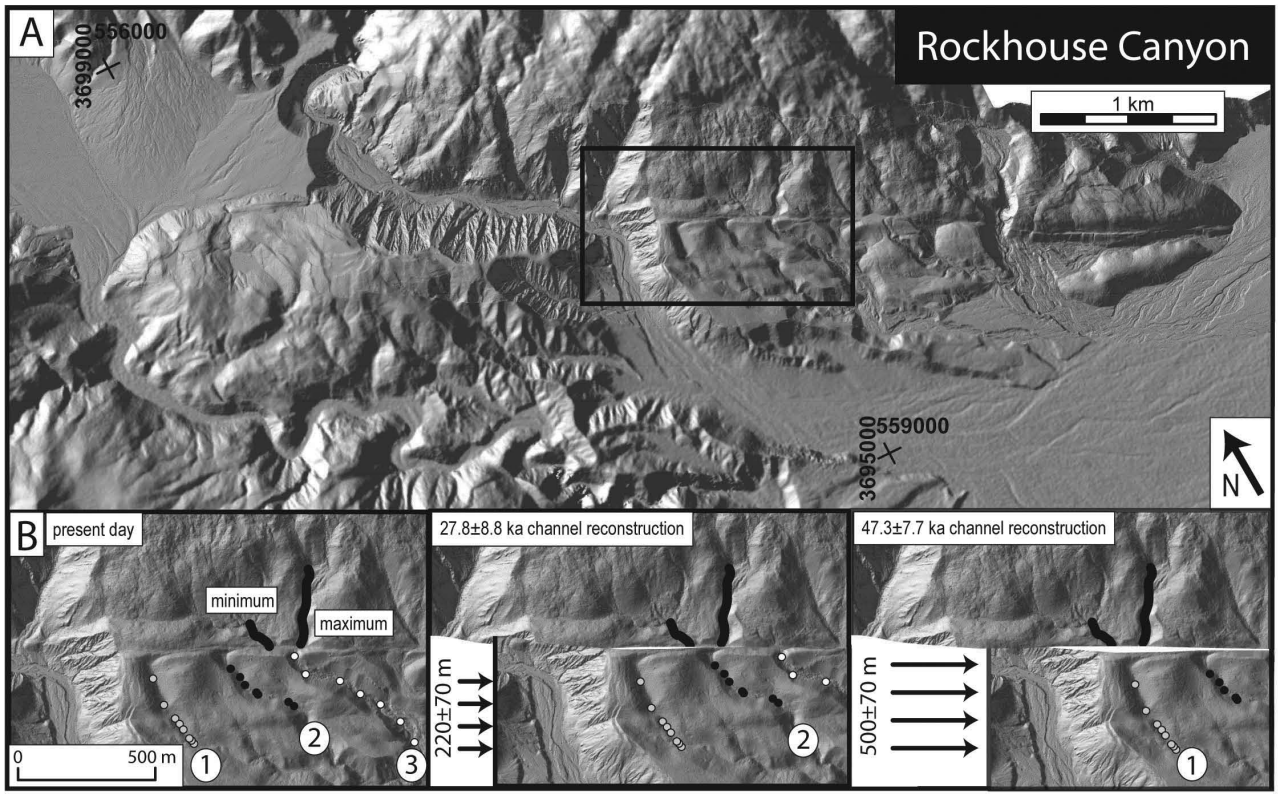
A
Rockhouse Canyon
3699000
556000
1 km
3695000
559000
N
B
present day
minimum
maximum
0
500 m
1
2
3
27.8±8.8 ka channel reconstruction
220±70 m
2
47.3±7.7 ka channel reconstruction
500±70 m
1

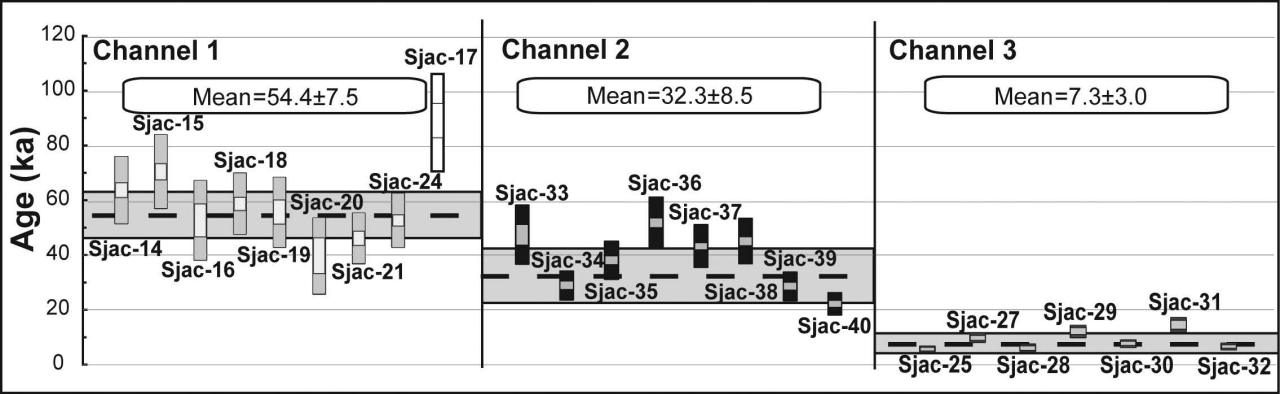
Age (ka)
120
100
80
60
40
20
0
Channel 1
Mean=54.4±7.5
Sjac-15
Sjac-17
Sjac-18
Sjac-24
Sjac-20
Sjac-14
Sjac-16
Sjac-19
Sjac-21
Channel 2
Mean=32.3±8.5
Sjac-33
Sjac-36
Sjac-37
Sjac-34
Sjac-39
Sjac-35
Sjac-38
Sjac-40
Channel 3
Mean=7.3±3.0
Sjac-27
Sjac-29
Sjac-31
Sjac-25
Sjac-28
Sjac-30
Sjac-32

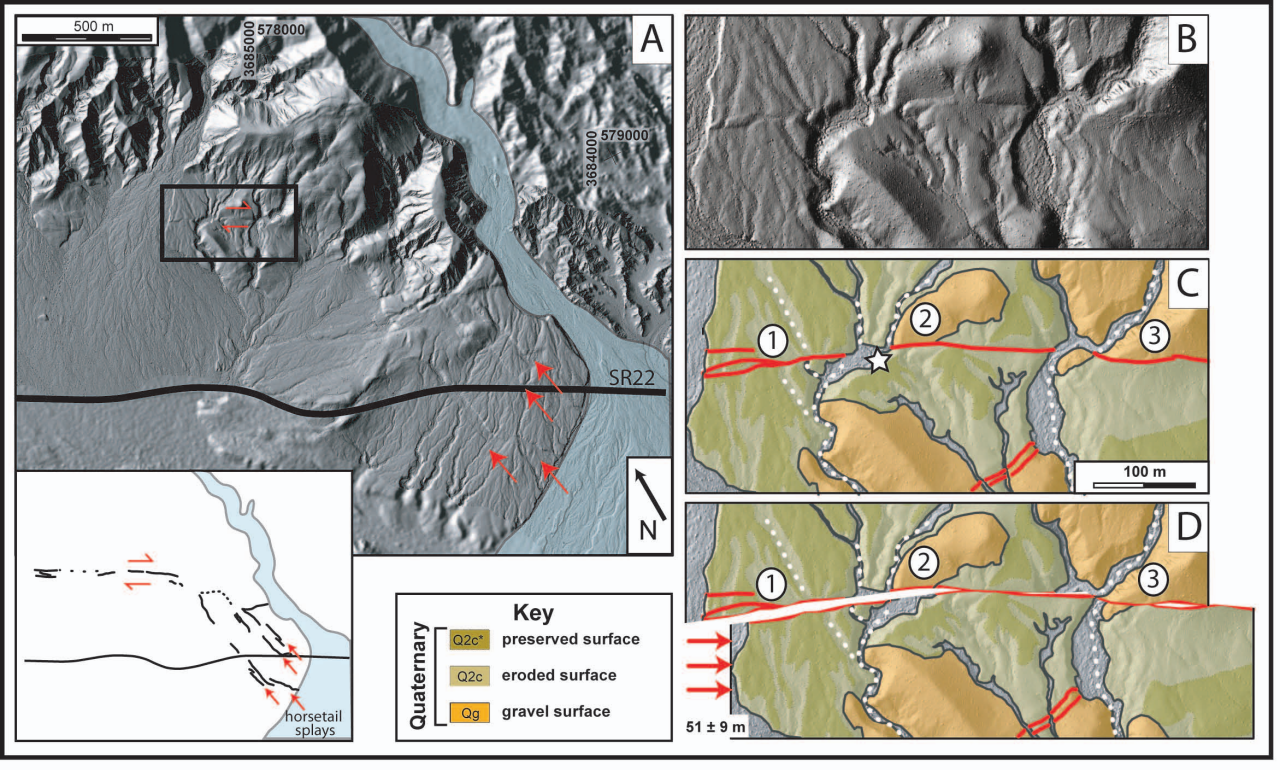
500 m
578000
3685000
579000
3684000
A
SR22
N
B
C
1
2
3
100 m
D
1
2
3
51 ± 9 m
horsetail
splays
Key
Quaternary
Q2c*
preserved surface
Q2c
eroded surface
Qg
gravel surface

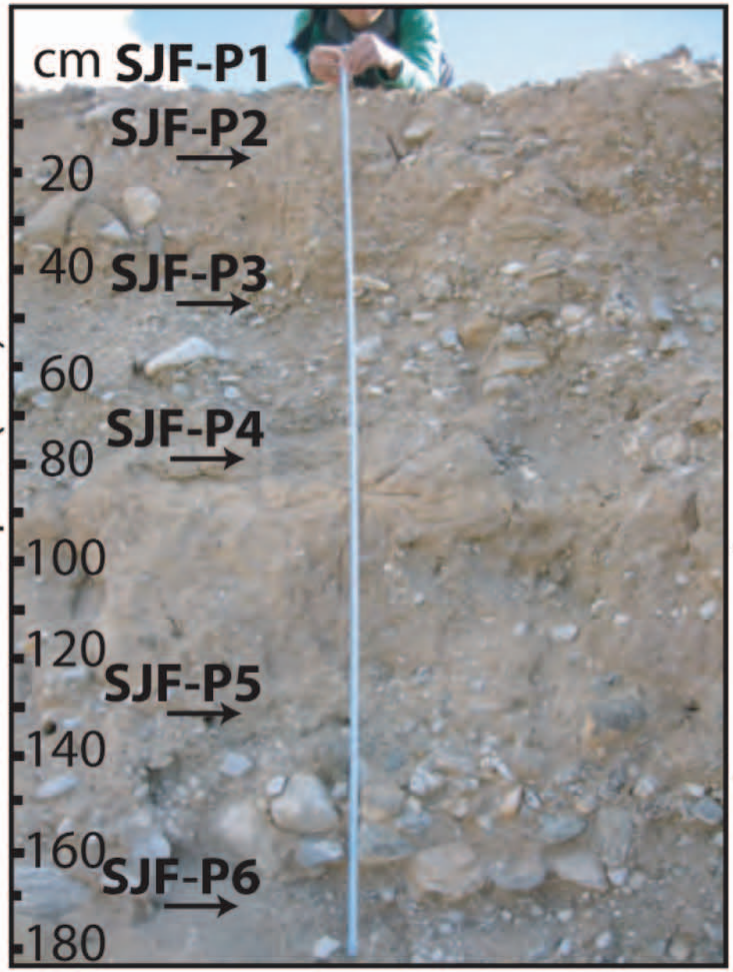
cm
SJF-P1
SJF-P2
20
40
SJF-P3
60
SJF-P4
80
100
120
SJF-P5
140
160
SJF-P6
180
depth (cm)

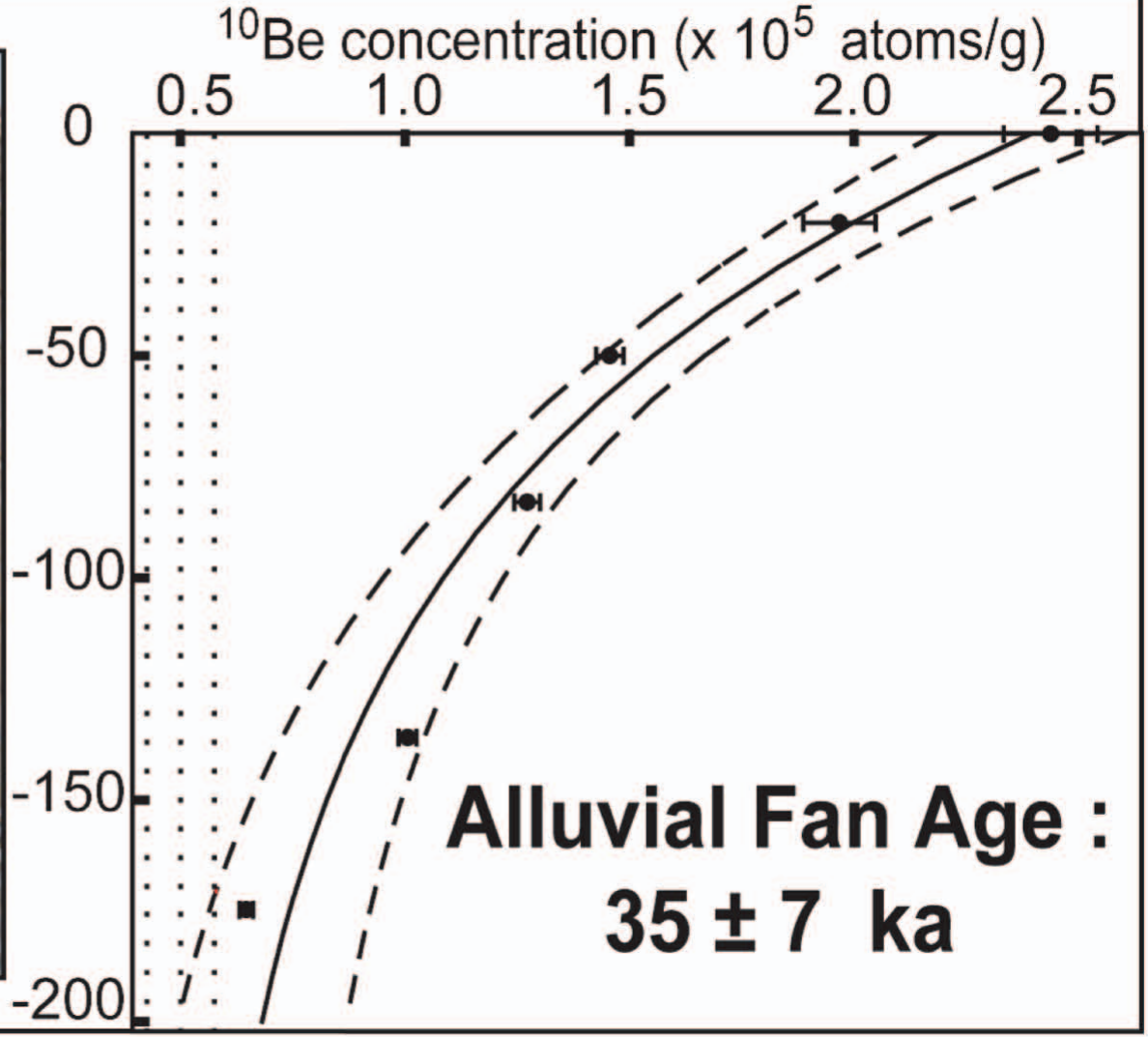
^{10}Be concentration (x 10^5 atoms/g)
0.5
1.0
1.5
2.0
2.5
0
-50
-100
-150
-200
Alluvial Fan Age :
35 ± 7 ka